OXFORD

Human Molecular Genetics, 2015, Vol. 24, No. 21 6080–6092

doi: 10.1093/hmg/ddv320
Advance Access Publication Date: 5 August 2015
Original Article

ORIGINAL ARTICLE

Haploinsufficiency for either one of the type-II regulatory subunits of protein kinase A improves the bone phenotype of *Prkar1a*$^{+/-}$ mice

Sisi Liu[1], Emmanouil Saloustros[1], Edward L. Mertz[2], Kitman Tsang[1], Matthew F. Starost[3], Paraskevi Salpea[1], Fabio R. Faucz[1], Eva Szarek[1], Maria Nesterova[1], Sergey Leikin[2] and Constantine A. Stratakis[1,*]

[1]Section on Endocrinology and Genetics (SEGEN), Program on Developmental Endocrinology & Genetics (PDEGEN), Eunice Kennedy Shriver National Institute of Child Health and Human Development (NICHD), [2]Section on Physical Biochemistry, Office of the Scientific Director, Eunice Kennedy Shriver National Institute of Child Health and Human Development (NICHD) and [3]Office of Research Services (ORS), Division of Veterinary Resources (DVR), Office of the Director (OD), National Institutes of Health (NIH), Bethesda, MD 20892, USA

*To whom correspondence should be addressed at: Section on Endocrinology and Genetics (SEGEN), Program on Developmental Endocrinology & Genetics (PDEGEN), *Eunice Kennedy Shriver* National Institute of Child Health and Human Development (NICHD), National Institutes of Health (NIH), Bethesda, MD 20892, USA. Tel: +1 3014964686; Fax: +1 3014020574; Email: stratakc@mail.nih.gov

Abstract

Carney Complex (CNC), a human genetic syndrome predisposing to multiple neoplasias, is associated with bone lesions such as osteochondromyxomas (OMX). The most frequent cause for CNC is PRKAR1A deficiency; *PRKAR1A* codes for type-I regulatory subunit of protein kinase A (PKA). *Prkar1a*$^{+/-}$ mice developed OMX, fibrous dysplasia-like lesions (FDL) and other tumors. Tumor tissues in these animals had increased PKA activity due to an unregulated PKA catalytic subunit and increased PKA type II (PKA-II) activity mediated by the PRKAR2A and PRKAR2B subunits. To better understand the effect of altered PKA activity on bone, we studied *Prkar2a* and *Prkar2b* knock out (KO) and heterozygous mice; none of these mice developed bone lesions. When *Prkar2a*$^{+/-}$ and *Prkar2b*$^{+/-}$ mice were used to generate *Prkar1a*$^{+/-}$*Prkar2a*$^{+/-}$ and *Prkar1a*$^{+/-}$*Prkar2b*$^{+/-}$ animals, bone lesions formed that looked like those of the *Prkar1a*$^{+/-}$ mice. However, better overall bone organization and mineralization and fewer FDL lesions were found in both double heterozygote groups, indicating a partial restoration of the immature bone structure observed in *Prkar1a*$^{+/-}$ mice. Further investigation indicated increased osteogenesis and higher new bone formation rates in both *Prkar1a*$^{+/-}$*Prkar2a*$^{+/-}$ and *Prkar1a*$^{+/-}$*Prkar2b*$^{+/-}$ mice with some minor differences between them. The observations were confirmed with a variety of markers and studies. PKA activity measurements showed the expected PKA-II decrease in both double heterozygote groups. Thus, haploinsufficiency for either of PKA-II regulatory subunits improved bone phenotype of mice haploinsufficient for *Prkar1a*, in support of the hypothesis that the PRKAR2A and PRKAR2B regulatory subunits were in part responsible for the bone phenotype of *Prkar1a*$^{+/-}$ mice.

Received: June 17, 2015. **Revised and Accepted:** July 31, 2015

Introduction

Protein kinase A (PKA) is an important enzyme involved in the regulation of a number of cellular functions and biological processes; it is a holoenzyme composed of two regulatory and two catalytic subunits (1). Four regulatory subunits (R1α, R1β, R2α and R2β) and four catalytic subunits (Cα, Cβ, Cγ and Prkx) of PKA have been identified (1,2). The type of the enzyme is determined by the dimer of the regulatory subunits: PKA type I (PKA-I) is composed by R1α or R1β, whereas PKA type II (PKA-II) is composed by R2α or R2β (3). Binding of cyclic adenosine monophosphate (cAMP) to the regulatory subunits frees the catalytic subunits from the tetramer (4); the latter are then phosphorylating downstream targets as other serine-threonine kinases do (5).

Abnormal PKA activity leads to a number of human diseases including Carney complex (CNC), a multiple neoplasia syndrome, which is caused by mutations in *PRKAR1A*, the gene coding for the PKA regulatory subunit R1α (6,7). R1α is responsible for PKA-I activity in most tissues, including bone (1,2). We have previously generated a mouse with only one active *Prkar1a* allele (*Prkar1a*$^{+/-}$) that developed various tumors including schwannomas, thyroid, bone and other lesions, overlapping with neoplasms that are seen in patients with CNC, including osteochondromyxomas (OMX) (8). In these mice, and in other settings of R1α deficiency, neoplastic growth and/or cellular proliferation appeared to be due to decreased control of the PKA catalytic subunit by the deficient or absent regulatory subunit (9,10). However, when haploinsufficiency for the main PKA catalytic subunit Cα (*Prkaca*$^{+/-}$) was introduced into the *Prkar1a*$^{+/-}$ background, the double heterozygous mice had overall more bone tumors (11). These mice also developed fibrous dysplasia-like lesions (FDL) that were different from those seen in *Prkar1a*$^{+/-}$ mice. PKA investigations in *Prkar1a*$^{+/-}$ and *Prkar1a*$^{+/-}$ *Prkaca*$^{+/-}$ mice showed that PKA-I deficiency and an overall increase in PKA-II activity could be the culprit behind the FDL lesions and the higher and earlier occurrence of bone neoplasms, such as OMX (11).

To better understand the effect of PKA-II on bone structures, we obtained *Prkar2a* (12) and *Prkar2b* (13) knock out (KO) mice which were used to generate the respective heterozygous mice and their double heterozygous counterparts, *Prkar1a*$^{+/-}$*Prkar2a*$^{+/-}$ and *Prkar1a*$^{+/-}$*Prkar2b*$^{+/-}$, after mating them with the *Prkar1a*$^{+/-}$ mouse. Caudal vertebrae lesions similar to those in *Prkar1a*$^{+/-}$ mice were found in all groups; however, newly formed bone material inside the lesions appeared more mature, with improved mineralization and organization, in *Prkar1a*$^{+/-}$ mice with either R2a or R2b deficiency. The data demonstrate that haploinsufficiency for either one of the type-II regulatory subunits improved the bone phenotype of mice haploinsufficient for *Prkar1a*, and support the hypothesis that PKA-II activity was in part responsible for the bone phenotype of *Prkar1a*$^{+/-}$ mice.

Results

Bone lesions in Prkar1a$^{+/-}$Prkar2a$^{+/-}$ and Prkar1a$^{+/-}$ Prkar2b$^{+/-}$ mice

As previously reported, schwannomas, thyroid tumors and bone lesions were found in *Prkar1a*$^{+/-}$ mice (8). Caudal vertebrae lesions, both OMX and FDL, were found in both *Prkar1a*$^{+/-}$ *Prkar2a*$^{+/-}$ and *Prkar1a*$^{+/-}$*Prkar2b*$^{+/-}$ mice, with single or multiple vertebral bodies containing these fibro-osseous neoplasms (Fig. 1A). The lesions became first noticeable at 6 months of age; they were present in 73.7% of *Prkar1a*$^{+/-}$*Prkar2a*$^{+/-}$ mice and 83.3% *Prkar1a*$^{+/-}$*Prkar2b*$^{+/-}$ by 12 months of age (Fig. 1B).

Histological examination by hematoxylin and eosin (H&E) staining (Fig. 1C) suggested that the fibro-osseous lesions started from the area adjacent to the growth plate and periosteal bone surface, as had been noted previously for *Prkar1a*$^{+/-}$ and *Prkaca*$^{+/-}$ *Prkar1a*$^{+/-}$ mice (11). At their earlier stages, lesions were more cellular with numerous blood vessels; osteoblasts and osteoclasts lined trabecular bone surfaces and the endosteum, indicating both active removal of the old and formation of new bone. Fibrous lesions then gradually filled the marrow space; their further expansion led to endosteal bone being rapidly resorbed and new periosteal bone deposited, along with the formation of new bone within the fibrous lesion. At later stages, bone lesions became less cellular, with fewer blood vessels, and some necrosis.

Bone organization, mineralization and new bone formation

Bright-field and polarized images of 10–15 μm cryosections of affected vertebrae were captured in a confocal Raman microscope followed by Raman micro-spectroscopic measurement of mineral: matrix ratios at different distances from the periosteal bone surface (Fig. 2). Well-organized osteocyte lacunae and collagen matrix as well as a narrow width of incompletely mineralized bone at the periosteal surface were consistent with mature lamellar bone in the cortical layer of wild-type animal vertebrae. Similar bone organization and mineralization was observed in unaffected vertebrae from mutant animals. Cortical bone layers surrounding late stage lesions in *Prkar1a*$^{+/-}$ mice were undermineralized and had disorganized osteocytes and collagen matrix. The structure of these regions was reminiscent of FDL lesions and consistent with the immature bone formation that we described in *Prkar1a*$^{+/-}$*Prkaca*$^{+/-}$ mice (11).

Surprising quilts of orthogonally oriented 50–100 μm patches of newly formed bone were observed only in *Prkar1a*$^{+/-}$*Prkar2a*$^{+/-}$ lesions. Good organization and mineralization of the matrix within these patches suggested a partial rescue of the bone structure at distance scales smaller than the patch size. In some of the patches, collagen fibers were oriented parallel to the bone surface, as expected in normal lamellar or fine-fibered bone. Other patches were perpendicular to the bone surface, reminiscent of collagen orientation in Sharpey fibers (14); yet, we did not observe distinct individual fibers expected within the latter bone formations. The quilted pattern of the patches and matrix organization within them appeared to be different from any other previously described bone matrix structure.

Newly formed cortical bones covering *Prkar1a*$^{+/-}$*Prkar2b*$^{+/-}$ lesions had well organized lamellar structure at all distance scales, which was parallel to the bone surface. However, these bones were undermineralized. The more gradual increase in the mineral:matrix ratio away from the periosteal surface, compared with wild-type bone, as well as the smaller thickness of the cortical layer suggested rapid bone formation on the periosteal side and resorption on the endosteal side, typically observed in much younger animals.

New bone formation in the lesions was examined by injections of calcein, which binds to and labels regions of active bone deposition in live animals (15,16) (Fig. 3). Little bone material (Fig. 3A) and little new bone formation (Fig. 3B and D) were observed in the marrow cavity of *Prkar1a*$^{+/-}$ vertebrae occupied by mostly FDL lesions. Much more bone material and more extensive deposition of new mineralized matrix were revealed by extensive calcein labeling of lesions in both *Prkar1a*$^{+/-}$*Prkar2a*$^{+/-}$ and *Prkar1a*$^{+/-}$*Prkar2b*$^{+/-}$ vertebrae. The larger distance between two fluorescent lines at the periosteal surface of cortical bone

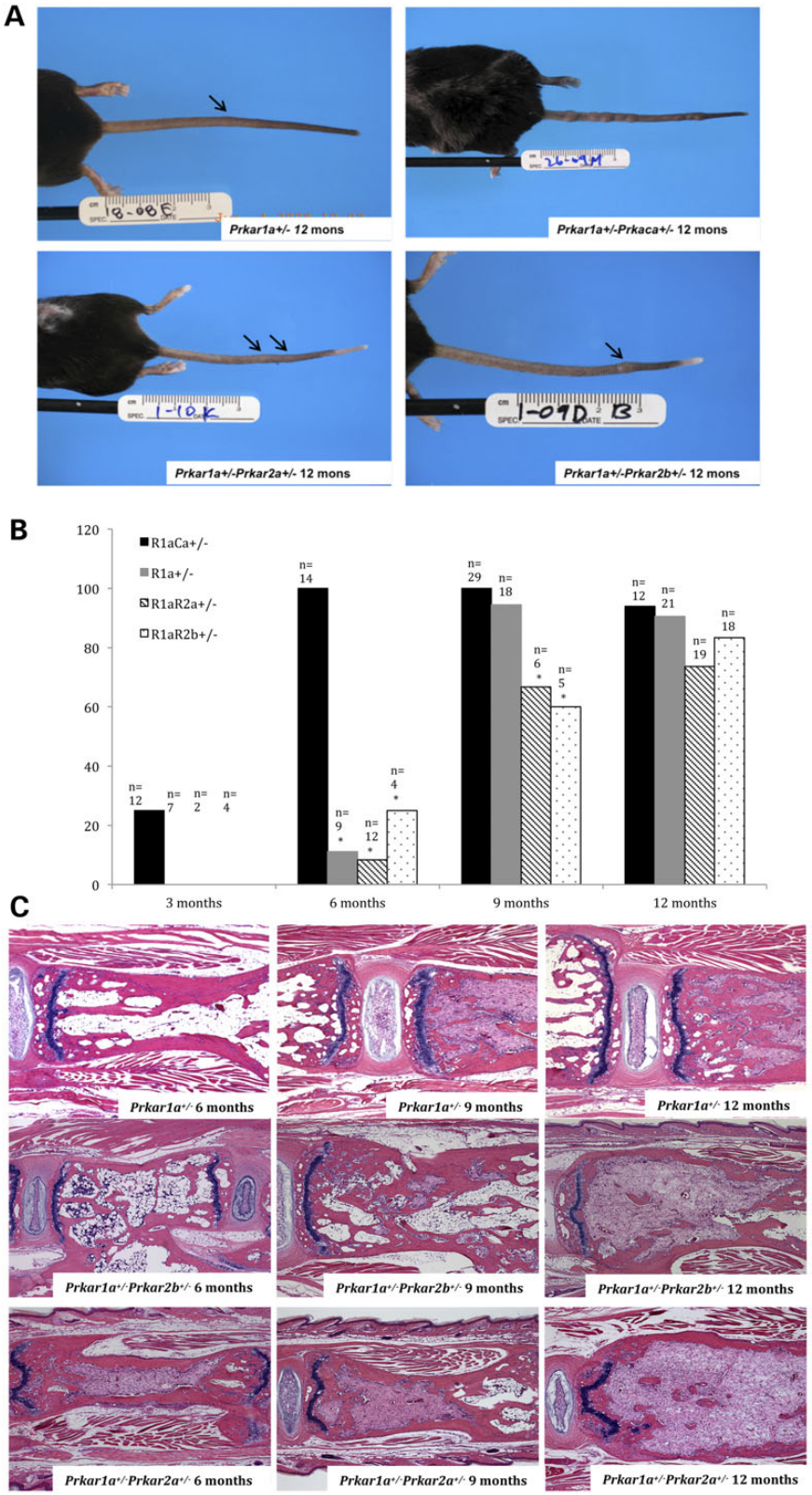

Figure 1. Development of bone lesions along the tails of *Prkar1a*$^{+/-}$, *Prkar1a*$^{+/-}$*Prkaca*$^{+/-}$, *Prkar1a*$^{+/-}$*Prkar2a*$^{+/-}$ and *Prkar1a*$^{+/-}$*Prkar2b*$^{+/-}$ mice. (**A**) Bone lesion status of the tails in 12-month-old mice. Tail bone lesions were found in mice with all four genotypes. The time of onset, number and malignancy of the tumors are different among different genotypes. (**B**) The percentages of mice with bone lesions at 6 months, 9 months and 12 months for each genotype. There is an earlier onset of tumors in *Prkar1a*$^{+/-}$*Prkaca*$^{+/-}$ mice (which are only presented here for comparison, since the data have been published previously) and a later onset in *Prkar1a*$^{+/-}$*Prkar2a*$^{+/-}$ and *Prkar1a*$^{+/-}$*Prkar2b*$^{+/-}$ mice; the latter have more tumors than both *Prkar1a*$^{+/-}$ and *Prkar1a*$^{+/-}$*Prkar2a*$^{+/-}$ mice at 6 months (**C**). Hematoxylin and eosin (H&E) staining of the caudal vertebrae with bone lesions. The lesions start at 6 months age and gradually fill the marrow space with time.

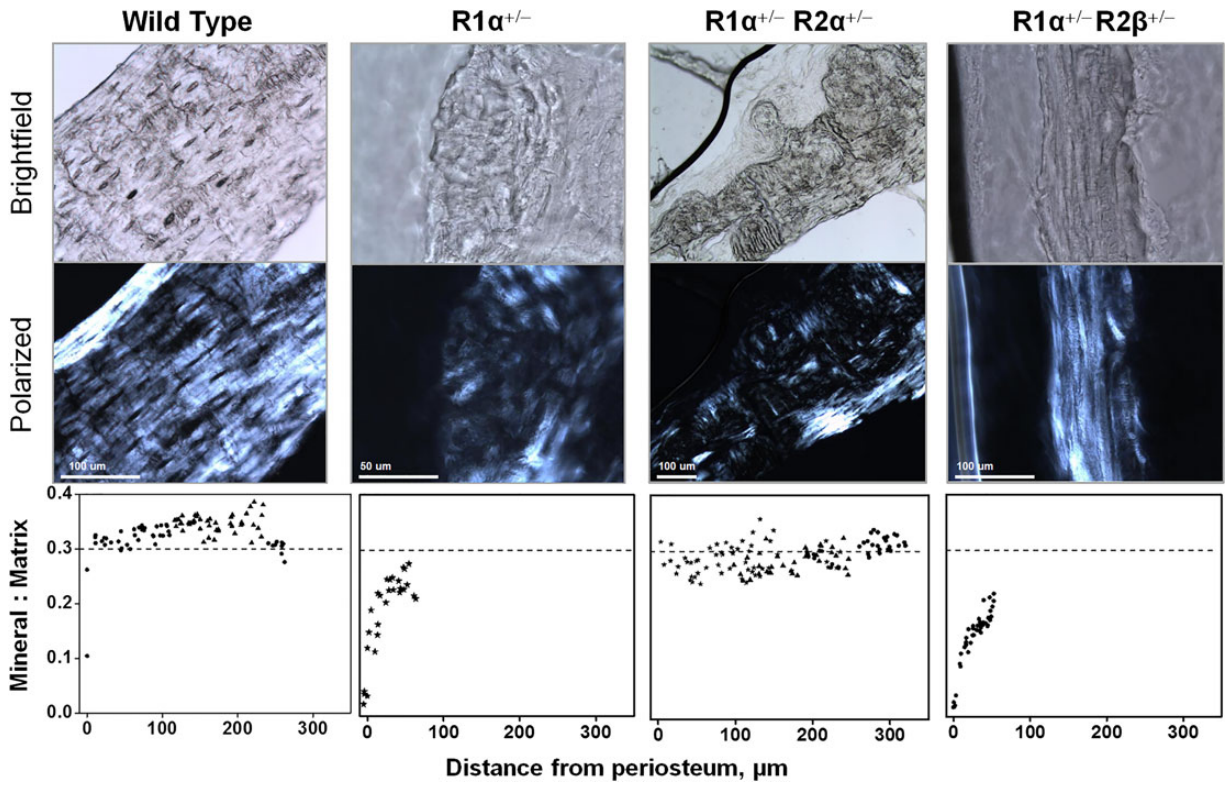

Figure 2. Organization and mineralization of cortical bone in tail vertebrae of wild-type animals and in affected tail vertebrae of animals with defective PKA activity. Bright-field (top panels) and polarized (middle panels) images were captured in a Raman confocal microscope, followed by Raman spectra measurements in the bone matrix outside osteocyte lacunae. The mineral:matrix ratios across the cortical bone (bottom panels) were calculated from the Raman spectra.

(Fig. 3C) indicates deposition of more bone matrix between two calcein injections and therefore overall faster bone formation in *Prkar1a*$^{+/-}$*Prkar2a*$^{+/-}$and *Prkar1a*$^{+/-}$*Prkar2b*$^{+/-}$ compared with *Prkar1a*$^{+/}$ mice. Calcein labeling inside the marrow space (Fig. 3D) also demonstrated more extensive formation and faster deposition of bone within *Prkar1a*$^{+/-}$*Prkar2a*$^{+/-}$ and *Prkar1a*$^{+/-}$*Prkar2b*$^{+/-}$ compared with *Prkar1a*$^{+/-}$ lesions.

Expression of osteoblastic markers in bone lesions

We performed immunohistochemistry staining of bone lesions for RUNX2, osterix, osteocalcin and DMP1, which are often used as markers of different stages in osteoblast differentiation (17–20). More pronounced nuclear localization of RUNX2 in osteoblastic cells lining the sites of active bone formation was found in tumors from double heterozygous compared with *Prkar1a*$^{+/-}$ animals (Fig. 4A). In the fibrous tissue away from bone surfaces, only a small fraction of *Prkar1a*$^{+/-}$ cells with fibroblast morphology were RUNX2-positive. A significantly larger fraction of such cells was RUNX2-positive in double heterozygous lesions; the most prominent nuclear localization of RUNX2 was observed in *Prkar1a*$^{+/-}$*Prkar2b*$^{+/-}$ cells.

Pronounced nuclear staining for osterix was observed in bone surface osteoblasts of all three genotypes (Fig. 4B). No nuclear localization and only a few cells with cytoplasmic osterix staining were observed in cells away from bone surfaces in *Prkar1a*$^{+/-}$ tumors, while a significant fraction of fibroblast-like cells in double heterozygous tumors had clear osterix staining with at least partial nuclear localization.

Similarly, pronounced osteocalcin staining was observed in bone surface cells that had osteoblast morphology in all three genotypes (Fig. 4C). No fibroblastic tumor cells appeared to be osteocalcin positive in *Prkar1a*$^{+/-}$ mice, while staining was observed in a significant fraction of double heterozygous tumor cells.

In *Prkar1a*$^{+/-}$ tumors, a significant fraction of osteocytes had unexpectedly light or no DMP1 staining (Fig. 4D) and bone surface osteoblasts had predominantly cytoplasmic staining. In *Prkar1a*$^{+/-}$ *Prkar2a*$^{+/-}$ tumors, the DMP1 staining pattern was different: most osteocytes had the expected intense staining and bone surface osteoblasts had pronounced nuclear and lighter cytoplasmic staining. In *Prkar1a*$^{+/-}$*Prkar2b*$^{+/-}$ tumors, we observed an intermediate staining pattern.

We also analyzed expression of alkaline phosphatase (ALP), osterix, osteocalcin and RUNX2 in cultured tumor cells by flow cytometry (Fig. 5A). After normalization of the mean fluorescence intensities to unstained controls, increased signals were found in double heterozygous tumor cells for all of these osteroblast markers, except for osteocalcin in *Prkar1a*$^{+/-}$*Prkar2b*$^{+/-}$ mice (Fig. 5B). This indicates a higher expression of most of the osteoblastic markers in double heterozygous tumor cells compared with *Prkar1a*$^{+/-}$ ones.

PKA isoform analysis

We performed diethylaminoethyl (DEAE) cellulose ion-exchange column chromatography on proteins extracted from tumors dissected from tails and measured PKA activity in different chromatographic fractions (21). The activity without cAMP was subtracted from the activity with cAMP as the baseline, so that the signal represented the amount of PKA in the chromatographic fraction that can be activated by cAMP (21,22). All three genotypes had a similar PKA isozyme pattern, with the first peak

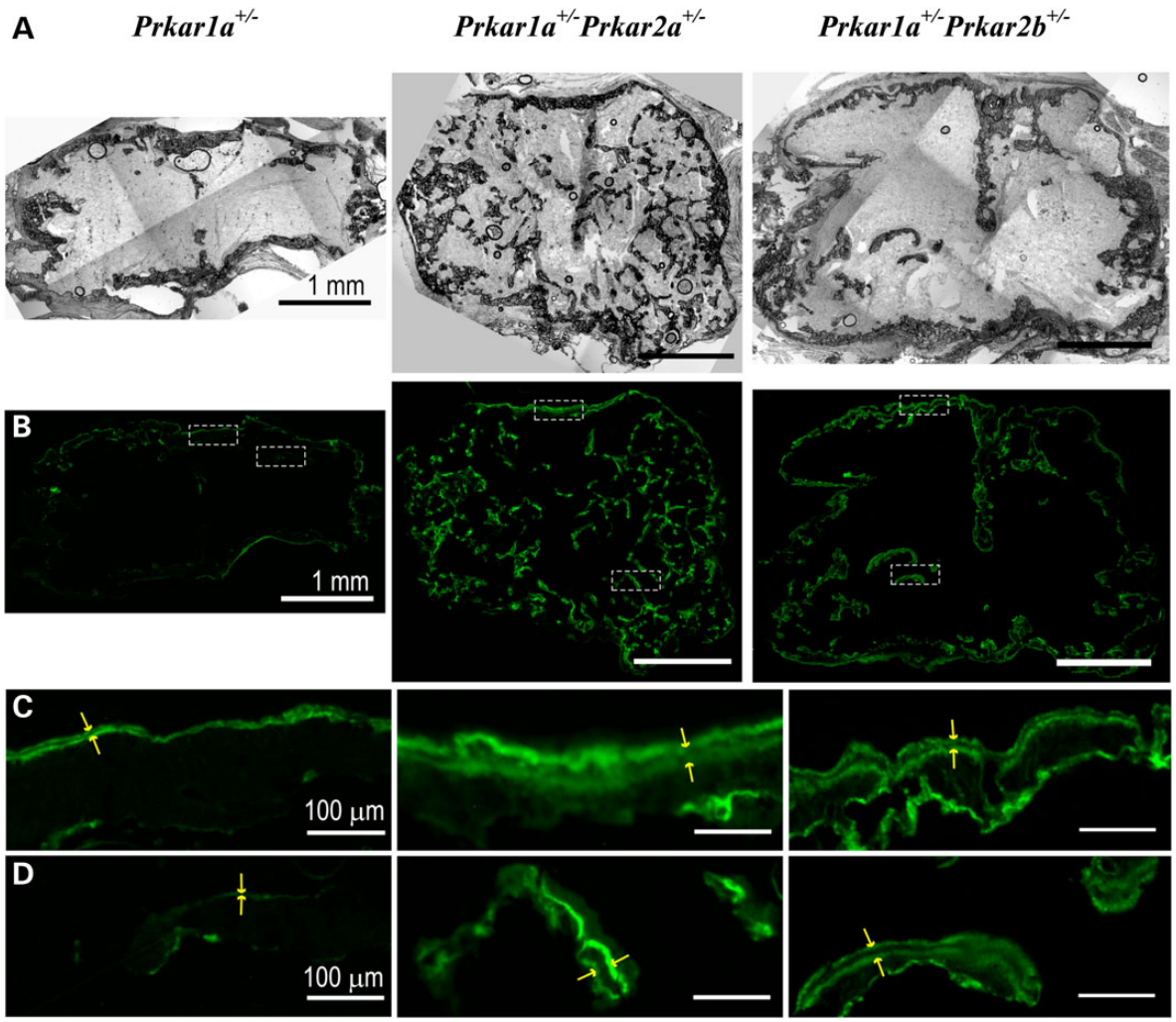

Figure 3. Mineralized bone matrix deposition in vertebral lesions. (**A**) Bright-field images. The mineralized matrix appears dark. (**B**) Calcein fluorescence of bone deposited at the time of two calcein injections. Rectangles mark the regions zoomed in C and D panels. (**C**) Calcein fluorescence images of cortical bone regions. (**D**) Calcein fluorescence of bone located inside the marrow cavity occupied by fibrous tumor tissue. Distance between the calcein labels indicated by double arrows is proportional to rate of bone matrix deposition.

representing cAMP-activatable PKA-I and the second peak representing cAMP-activatable PKA-II (21) (Fig. 6). As expected, decreased PKA-II to PKA-I ratios were found in *Prkar1a*$^{+/-}$*Prkar2a*$^{+/-}$ (PKA-II: PKA-I = 1.62, $P = 0.027$) and *Prkar1a*$^{+/-}$*Prkar2b*$^{+/-}$ tumors (PKA-II: PKA-I = 1.32, $P = 0.014$) compared with *Prkar1a*$^{+/-}$ (PKA-II: PKA-I = 1.82).

Expression of PKA subunits

Transcriptional and translational levels of PKA subunits in tumors were measured by quantitative real-time PCR (qPCR) analysis of mRNA and western blot (WB) analysis of proteins extracted from TRIzol tissue lysates. Quantitative real-time PCR measurement of Cα, Cβ, R1α, R2α and R2β mRNA levels revealed higher Cβ transcription in *Prkar1a*$^{+/-}$*Prkar2a*$^{+/-}$ ($2^{-\Delta\Delta Ct} = 3.5$, $P < 0.001$) and *Prkar1a*$^{+/-}$*Prkar2b*$^{+/-}$ ($2^{-\Delta\Delta Ct} = 2.3$, $P < 0.001$) relative to *Prkar1a*$^{+/-}$ tumors (Fig. 7). WB analysis of Cα, Cβ, Cγ and R1α was performed by utilizing GAPDH as control for normalizing relative band intensities (Fig. 8). Consistent with qPCR results, increased Cβ expression levels were found in *Prkar1a*$^{+/-}$*Prkar2a*$^{+/-}$ (2.5-fold increase) and *Prkar1a*$^{+/-}$*Prkar2b*$^{+/-}$ (4-fold increase) mouse tumors. Although there may be slight difference in Cα mRNA expression levels, this difference may be normalized by post-transcriptional and post-translational regulation mechanisms, leading to similar Cα protein levels in all genotypes.

Discussion

The importance of PKA and cAMP signaling in bone and cartilage development has been known for years (23–27): downstream of parathyroid hormone (PTH) and PTH-related protein (PTHrP), PKA signaling is stimulated by cAMP through Gsα's activation (28–30). In humans, mutations in *PRKAR1A* lead to OMX in the context of CNC (6), while activating mutations of Gsα subunit (coded by the *GNAS1* gene) were found in patients with FD in the context of McCune–Albright syndrome (MAS) (31,32). In this and previous studies, mice single or double heterozygous for PKA subunits were found to develop various bone tumors, including chondromas, OMX and rarely osteosarcomas (8,11,24). Interestingly, the same mice, in particular the *Prkar1a*$^{+/-}$*Prkaca*$^{+/-}$ one (11), developed FDL lesions reminiscent of humans with MAS (31,32), seen previously only in transgenic *Gnas1* mouse

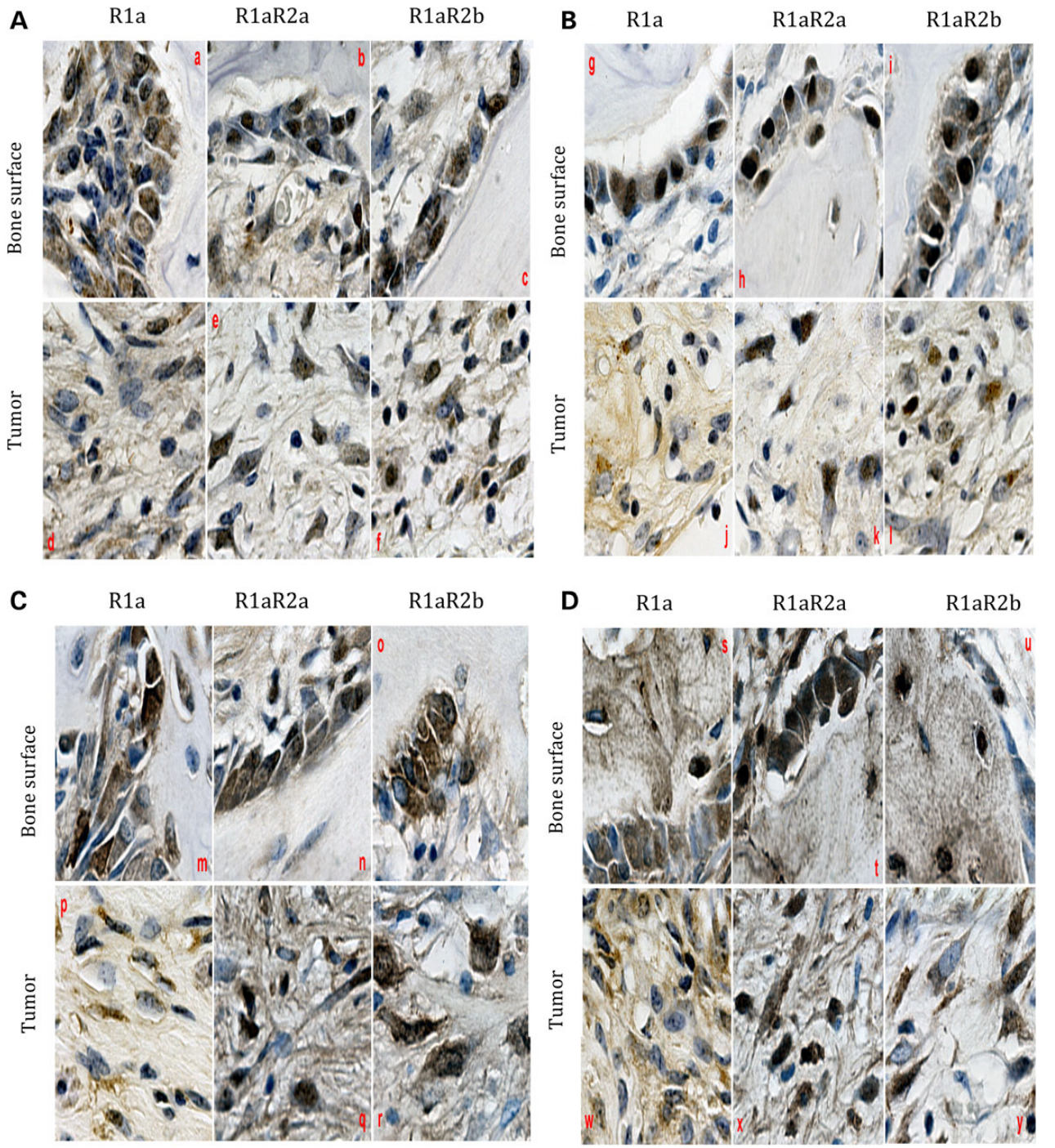

Figure 4. Expression of RUNX2 (**A**), osterix (**B**), osteocalcin (**C**) and DMP1 (**D**) at bone surfaces and within fibrous tumor tissue in vertebral lesions visualized by immunohistochemical (IHC) staining.

models (23). FDL lesions in PKA-defective mice filled the space of the marrow, mostly of caudal vertebrae, where normal cortical bone structure was destroyed and newly formed bone was immature and under-mineralized. As we described previously (11), abnormal PKA activity recruited adult bone marrow stromal cells (aBMSCs) to the bone lesions in *Prkar1a*$^{+/-}$ and, in particular the *Prkar1a*$^{+/-}$*Prkaca*$^{+/-}$ mice (11,24). These cells were unable to undergo the normal differentiation process, giving rise to immature osteoblasts that produced disorganized and under-mineralized bones (11). The increased PKA-II to PKA-I ratio in these animals (8,11) suggested that excess PKA-II activity might be responsible for at least part of the phenotype.

Indeed, in the present study, *Prkar1a*$^{+/-}$*Prkar2a*$^{+/-}$ and *Prkar1a*$^{+/-}$*Prkar2b*$^{+/-}$ double heterozygous mice developed bone lesions in the tails like *Prkar1a*$^{+/-}$ did. There was an overall better new bone formed in these mice compared with *Prkar1a*$^{+/-}$ mice partially reversing the abnormalities detected in the latter. There were also some interesting, genotype-specific findings,

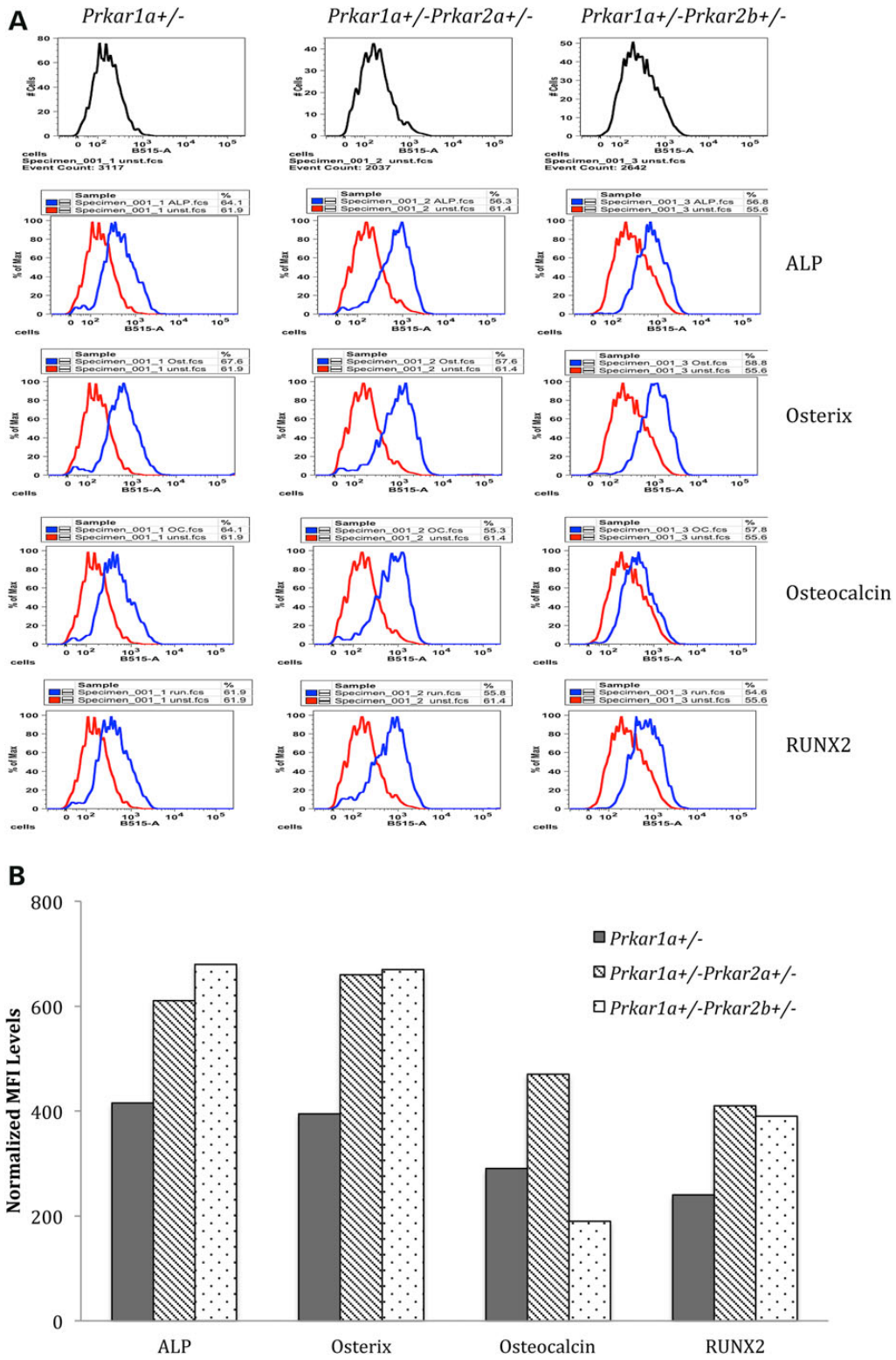

Figure 5. Flow cytometry analysis of the expression levels of osteoblast markers. (**A**) Histogram of cell counts versus log fluorescence. (**B**) Mean fluorescence intensity levels (MFI) normalized to unstained cells as controls. Increased expression levels of osteoblast markers were found in double heterozygous mice compared with *Prkar1a*$^{+/-}$ ones, except for osteocalcin in *Prkar1a*$^{+/-}$*Prkar2b*$^{+/-}$ mice.

like the unusual quilted bone structure in *Prkar1a*$^{+/-}$*Prkar2a*$^{+/-}$ mice, which has not been described before, to the best of our knowledge. Also, the *Prkar1a*$^{+/-}$*Prkar2b*$^{+/-}$ mice had more tumors than both *Prkar1a*$^{+/-}$ and *Prkar1a*$^{+/-}$*Prkar2a*$^{+/-}$ mice at 6 months (Fig. 1B), which may indicate that early on R2β deficiency may be contributing more to bone tumor formation.

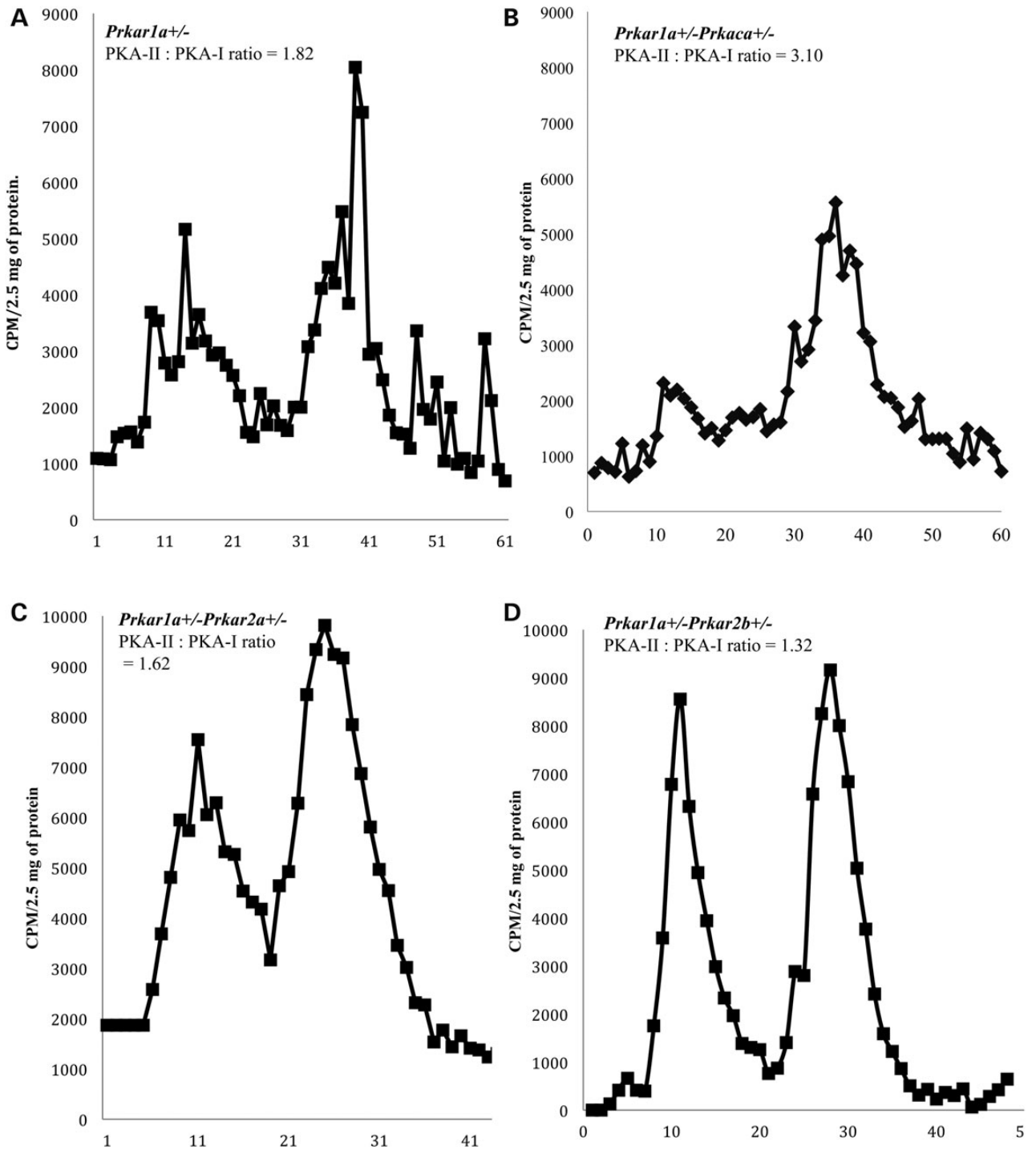

Figure 6. DEAE-chromatography of PKA isozymes in tail lesions: PKA-II to PKA-I ratio was calculated from the average intensities of 10 fractions within the peak. (**A**) *Prkar1a*$^{+/-}$ mice, PKA-II : PKA-I ratio = 1.82. (**B**) *Prkar1a*$^{+/-}$*Prkaca*$^{+/-}$ mice, PKA-II : PKA-I ratio = 3.10. (**C**) *Prkar1a*$^{+/-}$*Prkar2a*$^{+/-}$ mice, PKA-II : PKA-I ratio = 1.62. (C) *Prkar1a*$^{+/-}$ *Prkar2b*$^{+/-}$ mice, PKA-II: PKA-I ratio = 1.32.

Increased expression of ALP, RUNX2, osterix and osteocalcin indicated more advanced osteoblastic differentiation in both double heterozygous animal lesions. Increased expression of ALP, which hydrolyzes pyrophosphate to facilitate bone mineralization, is normally observed at early stages of osteogenesis (33,34). RUNX2 is an essential factor in activating downstream osterix advancing osteogenesis (35–38); in a characteristic contrast with both PKA-I defective mice (*Prkar1a*$^{+/-}$ and *Prkar1a*$^{+/-}$*Prkarca*$^{+/-}$), both RUNX2 and osteocalcin (produced by more mature osteoblasts) were increased in PKA-II defective double heterozygous mice. A particularly important observation was the significant progression of a large fraction of tumor cells located away from bone surfaces toward osteoblasts in both *Prkar1a*$^{+/-}$*Prkar2a*$^{+/-}$ and *Prkar1a*$^{+/-}$*Prkar2b*$^{+/-}$ animals. These cells appear to be responsible for the much more extensive initiation of new bone formation and subsequent faster deposition of bone material inside

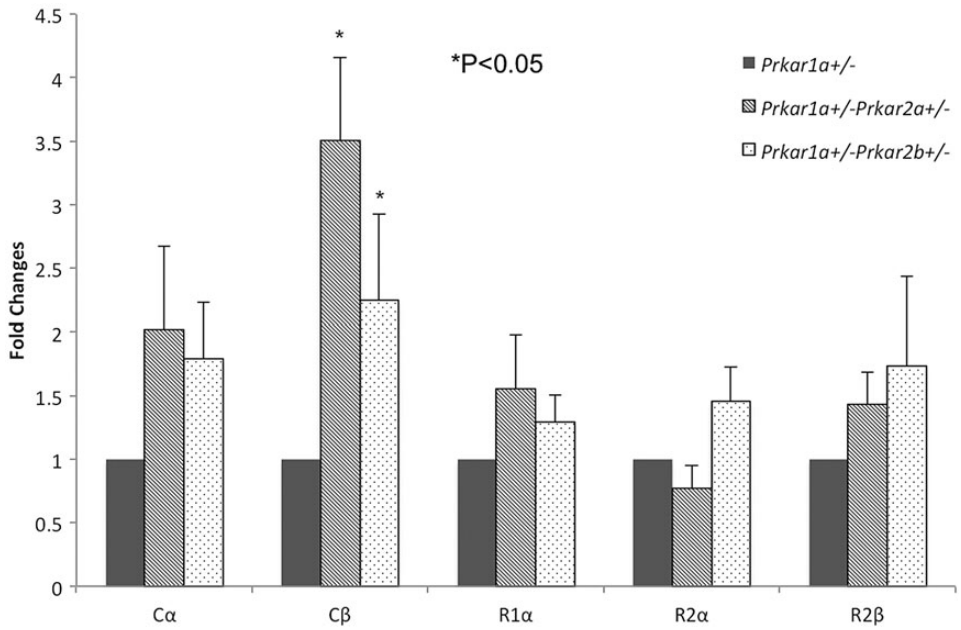

Figure 7. Quantitative real-time PCR analysis of mRNA expression levels of PKA subunits: Cα, Cβ, R1α, R2α and R2β in different genotypes. Relative fold expression levels of each subunit in the double heterozygous lesions to that in *Prkar1a*$^{+/-}$ are represented by $2^{-\Delta\Delta Ct}$. *Prkar1a*$^{+/-}$ was set as standard with $2^{-\Delta\Delta Ct}$ equals 1. Error bars represent means ± SEM. *, $P < 0.05$.

the FDL lesions filling the marrow cavity in these animals compared with both *Prkar1a*$^{+/-}$ and *Prkar1a*$^{+/-}$*Prkarca*$^{+/-}$ mice.

Pronounced expression and nuclear localization of DMP1 in many of the double heterozygous FDL cells might indicate that their differentiation is akin to that of embryonic rather than "older" adult osteoblasts. DMP1, besides being a nuclear transcription factor, is a secreted protein, which is strongly expressed by embryonic osteoblasts and may be affecting significantly the microenvironment of the FDL lesions (39). In adult animals, DMP1 is expressed primarily by osteocytes and its localization within and outside the cells changes upon progression of osteoblasts to osteocytes (40–42). Significant differences in both the expression level and nuclear localization of DMP1 between all three genotypes suggested that PKA isozymes (and their switching) have important and distinct roles in this process.

There is evidence in different systems that PKA-I and PKA-II are responsible for regulating distinct downstream signaling pathways and cellular functions (1,43–47). In part, this appears to be through recruitment of different catalytic subunits. Among the four catalytic subunits (Cα, Cβ, Cγ and PRKX), Cα, coded by the *PRKACA* gene is the most frequently and highly expressed (48); however, Cβ, coded by the *PRKACB* gene, is also ubiquitously expressed, albeit at lower levels than *PRKACA*. Although Cβ appears to account for only 5–10% of total PKA activity in mouse cells (49–51), its importance increases in states of dysregulated PKA activity (49) and/or Cα deficiency (51) or under the presence of strain-specific genetic modifiers (50). Human studies recently pointed to different phenotypic effects of increased Cα (48,52,53) versus Cβ (54) expression. In both *Prkar1a*$^{+/-}$*Prkar2a*$^{+/-}$ and *Prkar1a*$^{+/-}$*Prkar2b*$^{+/-}$ animals, *Prkacb* RNA and PRKACB protein levels were increased, even though the *Prkaca* gene was intact. More studies are needed for better understanding of Cβ's function but both the data from the present investigation and the single human patient with skeletal defects and *PRKACB* gene copy number gain (54) indicate a possible role for Cβ in bone development, osteoblast differentiation and/or tumors.

In conclusion, PKA-II haploinsufficiency reversed some but not all of the bone effects of PKA-I defects. The individual subunits may confer different effects in skeletal development, as suggested by small but remarkable differences between R2α and R2β deficiency in the *Prkar1a*$^{+/-}$ background. There is now little doubt that osteogenesis is affected by relatively modest perturbations of the relative ratio between the two PKA isozymes, first suggested by the studies of the *Prkar1a*$^{+/-}$ (8) and *Prkar1a*$^{+/-}$*Prkarca*$^{+/-}$ mice (11). Why were there any bone lesions formed in *Prkar1a*$^{+/-}$*Prkar2a*$^{+/-}$ and *Prkar1a*$^{+/-}$*Prkar2b*$^{+/-}$mice? These mice still have unregulated Cα activity (due to R1α deficiency), as previously suggested (8–10,49); in addition, the present study shows that the Cβ catalytic subunit may have its own effects on osteogenic differentiation, and bone formation, organization or structure, as suggested also by the study of the single human patient with *PRKACB* amplification and skeletal defects (54). Regulation of PKA subunits expressions may be used therapeutically for CNC and other diseases, but we need to be aware of the toxicity effects this may cause to other systems.

Material and Methods

Generation of *Prkar1a*$^{+/-}$*Prkar2a*$^{+/-}$ and *Prkar1a*$^{+/-}$*Prkar2b*$^{+/-}$ double heterozygous mice

Prkar1a heterozygous mice (*Prkar1a*$^{+/-}$) were previously generated in our lab by deletion of exon 2 in one allele of *Prkar1a* (Prkar1a$^{\Delta 2}$) (7). B6.129X1-Prkar2a$^{tm1Gsm/Mmmh}$ *Prkar2a* knockout mice (*Prkar2a*$^{-/-}$) and B6.129X1-Prkar2b$^{tm1Gsm/Mmmh}$ *Prkar2b* knockout mice (*Prkar2b*$^{-/-}$) were purchased from Mutant Mouse Regional Resource Center (MMRRC). In *Prkar2a*$^{-/-}$ mice, a neomycin resistance cassette replaces the translation and transcription start site in exon 1 (11). In *Prkar2b*$^{-/-}$ mice, a neomycin resistance cassette replaces the coding region in exon 1 (43). *Prkar1a*$^{+/-}$ and *Prkar2a*$^{-/-}$ mice were interbred to generate *Prkar1a*$^{+/-}$*Prkar2a*$^{+/-}$ double heterozygous mice; *Prkar1a*$^{+/-}$ and *Prkar2b*$^{-/-}$ mice were

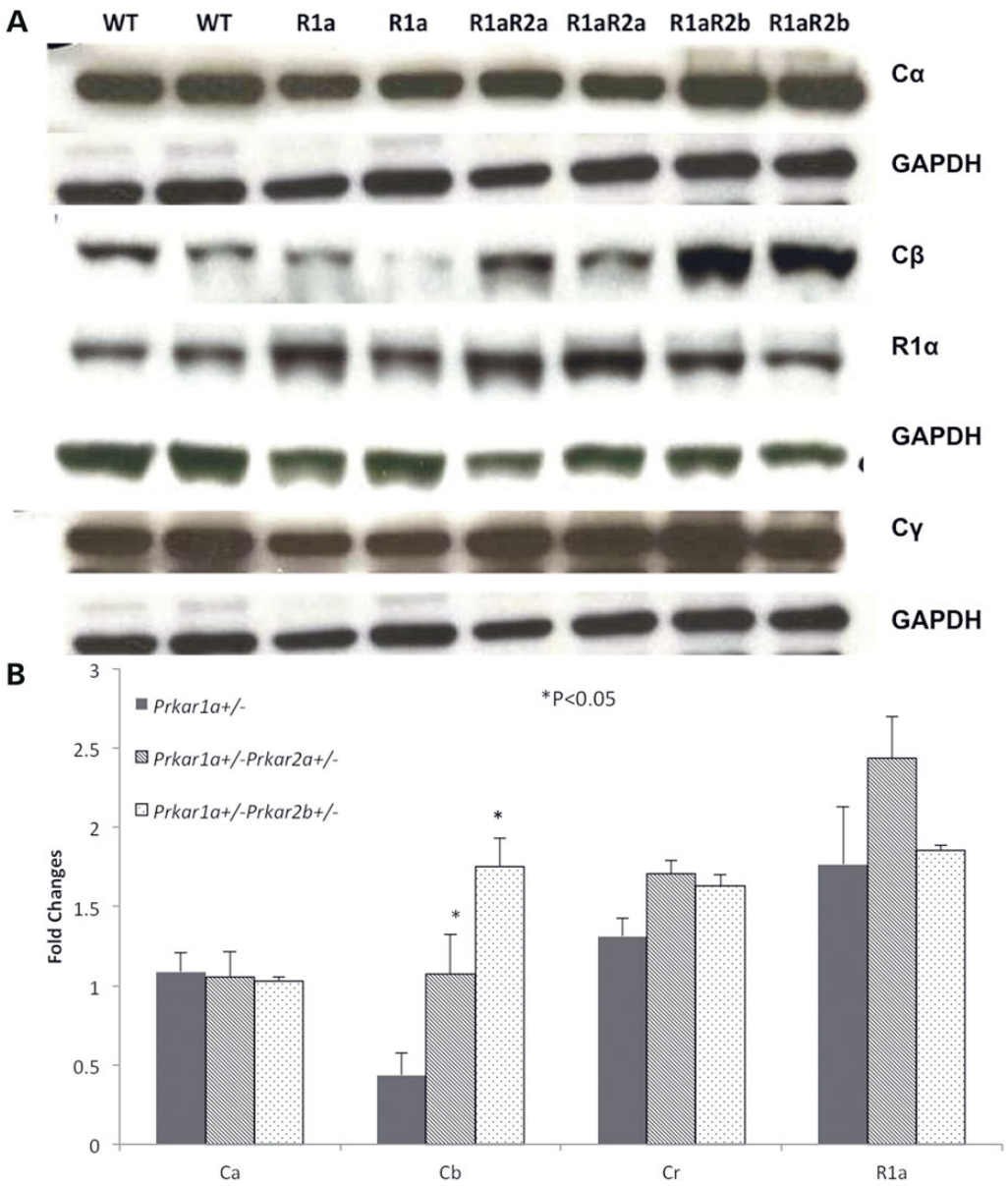

Figure 8. Western blot analysis of the expression levels of PKA subunits Cα, Cβ Cγ and R1α in bone lesions from different genotypes. (**A**) Bands of target proteins and corresponding Gapdh control after exposure. (**B**) Comparison of protein expression levels after normalization to Gapdh. Error bars represent means ± SEM. *, $P < 0.05$.

interbred to generate *Prkar1a*$^{+/-}$*Prkar2b*$^{+/-}$ double heterozygous mice. All mice were maintained on a C57BL/6 129Sv/B6 hybrid background. All animal-related studies were carried out under animal protocol 12–033 in 10A Animal Facility, NIH, Bethesda, MD, USA.

Genotyping analysis

Polymerase chain reaction (PCR) was used for genotyping. Three primers (5′-AGCTAGCTTGGCTGGACGTA-3′, 5′-AAGCAGGCGAG CTATTAGTTTAT-3′ and 5′-CATCCATCTCCTATCCCCTTT-3′) were used for *Prkar1a* genotyping; the WT allele generates a 250 base pair (bp) fragment, while the Prkar1a$^{\Delta 2}$ null allele generates a 180 bp product. Two pairs of primers were used for genotyping of *Prkar2a*; the first pair (5′-CAGCATGAGCCACATCCAGAT-3′ and 5′-GATGACGGGGACTGCGCTGGA-3′) amplifies the WT allele and generates a 220 bp product, while the second pair (5′-AGGTGG TCCTGTGTCACTTCA-3′ and 5′-GTGGTTTGTCCAAACTCATCAA TGT-3′) amplifies the neo-inserted allele and generates a 330 bp product. Genotyping of Prkar2b was also performed with two pairs of primers; the first pair (5′-GGCGAAGTTGACACCCTTA C-3′ and 5′-CTTCACGGTGGAGGTGCT-3′) identifies the WT allele with a product of 330 bp, while the second pair (5′-AGGAGCTGGA GATGCTGCCAA-3′ and 5′-GTGGTTTGTCCAAACTCATCAATGT-3′) identifies the neo-inserted allele with a product of 194 bp.

Hematoxylin and eosin (H&E) and other immunohistochemical (IHC) staining

Tail vertebrae with tumors were dissected from mice and fixed in 10% neutral buffered formalin for 24 h, followed by decalcification in 10% formic acid (Decalcifier I, Surgipath Medical Industries Inc., Richmond, IL, USA) for 24 h and rinsing in running water for 30 min. Fixed tissue was embedded into paraffin blocks, sectioned (5 μm) and H&E or IHC stained by Histoserv Inc.

(Germantown, MD, USA). IHC staining was performed with mouse primary antibodies for RUNX2, osteocalcin, osterix and DMP1 (all from Santa Cruz biotechnology, Inc., Dallas, TX, USA).

Raman microspectroscopy

Mice that were 12 to 16 months old (*Prkar1a*$^{+/-}$, *Prkar1a*$^{+/-}$ *Prkar2a*$^{+/-}$, and *Prkar1a*$^{+/-}$*Prkar2b*$^{+/-}$) with microscopically visible caudal vertebrae tumors were used; 15 μm mid-coronal and mid-sagittal cryosections of affected caudal vertebrae were washed with PBS and hydrated in sub-saturating CsCl, 10 mM HEPES, pH 7.4. Sections were placed between quartz slides and examined in a confocal Raman microscope (Senterra, Bruker Optics, Inc). 10X/0.3NA objective was used to generate bright-field and polarized images. To analyze mineralization levels, Raman spectra were collected from 1 × 1 μm spots within extracellular matrix away from osteocyte lacunae (40X/0.95NA objective, 50 μm pinhole and 532 nm/14 mW depolarized excitation laser). Mineral/matrix ratio was calculated to represent mineralization levels. After subtraction of peak baselines and water and quartz contributions, ratio of integral intensities of spectral peaks of v_1PO4^{3-} stretching vibration of mineral phosphate (922–983 cm^{-1}) and CH stretching vibrations in organic molecules (2820–3020 cm^{-1}) was calculated for each genotype.

Calcein injection studies

1X calcein solution was made by dissolving 3 mg calcein powder (Sigma-Aldrich, St. Louis, MO) in 1 ml 2% $NaHCO_3$ (0.2 g of $NaHCO_3$ in 10 ml double distilled H_2O, pH 7.4). Twelve months old mice with visible caudal vertebrae tumors were used for injection; each mouse was weighted, and 10 μg calcein was used per gram of body weight. Two subcutaneous calcein injections were performed, the first one on day 1 and the second one on day 6; mice after both injections were sacrificed one day after the second injection on day 7.

Primary tail tumor cell cultures

Bone tumors were dissected from tail vertebrae. Muscles and fibrous tissues were removed under a dissection microscope. Each tumor was chopped into 1–3 mm fragments, which were incubated with Collagenase I (Sigma-Aldrich, St. Louis, MO) at 37°C for 15 min, washed twice with PBS and cultured in one-well of a six-well plate with DMEM (Invitrogen, Carlsbad, CA, USA) containing 10% FBS (Hyclone, Logan, UT) and 1% Penicillin–Streptomycin (Invitrogen, Carlsbad, CA, USA) for 7 days. Cells that migrated out of the tumor fragments were detached by 0.05% Trypsin-EDTA (Invitrogen, Carlsbad, CA, USA), transferred into a 75 cm^2 flask and grown to confluence; media was refreshed every 3 days. These primary cells were used for fluorescence-activated cell sorting (FACS) analysis.

RNA and protein extraction from tumors by TRIzol

Tail tumors were dissected from vertebrae, snap frozen in liquid nitrogen and kept at −80°C before processing. The tissue was homogenized in 1 ml TRIzol (Invitrogen, Carlsbad, CA, USA) per 100 mg using a Polytron homogenier (Thermo Fisher Scientific Inc., Waltham, MA, USA). RNA and proteins were isolated following the standard TRIzol protocol (Invitrogen, Carlsbad, CA, USA) RNA was dissolved in RNase-free water and analyzed in NanoDrop 2000 (Thermo Fisher Scientific Inc., Waltham, MA, USA) to determine its concentration and quality.

DEAE-cellular chromatography

The DEAE-cellular chromatography was performed as described (21). Briefly, DEAE column was pre-equilibrated with buffer containing 10 mM Tris/HCl, pH7.1, containing 1 mM EDTA and 1 mM phenylmethylsulfonyl fluoride (EMD Biosciences, La Jolla, CA, USA). For each sample, 2.5 mg of protein was loaded to the column; the column was washed with 30 ml buffer and eluted with a 0–350 mM NaCl gradient at a flow rate of 15 ml/h. A total of 2 ml fractions were collected on ice and assayed for protein kinase activity.

Quantitative real-time PCR (qPCR)

For each sample, 1 μg of mRNA was reverse transcribed to cDNA using High Capacity RNA-to-cDNA Kit (Applied Biosystems, Foster City, CA, USA). Quantitative real-time PCR was performed in an Applied Biosystems 7500 real-time PCR system. mRNA expression levels of PKA subunits were detected by *Prkaca* (Mm00660092_m1), *Prkacb* (Mm01312555_m1), *Prkar1a* (Mm00660315_m1), *Prkar2a* (Mm00435916_m1) and *Prkar2b* (Mm01293022_m1) Taqman Gene Expression Assays (Applied Biosystems, Foster City, CA, USA). Gene expression levels were normalized to Taqman Rodent *Gapdh* control, (Applied Biosystems, Foster City, CA, USA). Gene expression in double heterozygous mice was calculated relative to *Prkar1a*$^{+/-}$ using $2^{-\Delta\Delta Ct}$ values (55).

Western blot analysis

Protein concentrations were measured by BCA protein assay (Thermo Fisher Scientific Inc., Waltham, MA, USA). For each sample, 30 μg protein was mixed with 2X SDS gel loading buffer, boiled for 5 min and loaded into a 10% Tris-glycine gel. After running the gel at 100 V for 2.5 h, proteins were transferred to a nitrocellulose membrane. The membrane was blocked with 5% nonfat milk in TBS-Tween (TBST). Target proteins were detected by the following primary antibodies: cα (Santa cruz biotechnology, Inc., Dallas, TX, USA), Cβ (Santa cruz biotechnology, Inc., Dallas, TX, USA), R1α (Santa cruz biotechnology, Inc., Dallas, TX, USA), R2α (Santa cruz biotechnology, Inc., Dallas, TX, USA) and R2β (Santa cruz biotechnology, Inc., Dallas, TX, USA), and peroxidase-conjugated secondary antibodies against rabbit IgG (Jackson ImmunoResearch Laboratories, Inc. West Grove, PA, USA). All antibodies were diluted in 5% nonfat milk in TBST. Signals were detected by Western Lightning Enhanced Luminol Reagent (PerkinElmer, Santa Clara, CA, USA). Images of the gels were captured in a Kodak X-OMAT 2000A processor (S&W Imaging, Frederick, MD, USA) and quantitatively analyzed with Image J software (23) (NIH, Bethesda, MD, USA).

Fluorescence-activated cell sorting

Cells (1 × 10^6) were detached from 75 cm^2 flasks using 0.05% trypsin-EDTA (Invitrogen, Carlsbad, CA, USA), collected into 5 ml polystyrene round-bottom tubes, washed twice with PBS containing 2% FBS and resuspended in 100 μl PBS with 2% FBS. The cells were permeabilized by incubating with 300 μl Cytofix/Perm at room temperature for 20 min. Alkaline phosphatase, osterix, osteocalcin and RUNX2 antibodies (all from Santa Cruz biotechnology, Inc., Dallas, TX, USA) were conjugated to Alexa Fluor 488, Alexa Fluor 594, Alexa Fluor 680 and pacific blue fluorochromes respectively using the Zenon Rabbit IgG labeling Kit (Life Technologies, Grand Island, NY, USA). Briefly, 1 μg of antibody was mixed with 5 μl of Zenon rabbit IgG labeling reagent and incubated for 5 min at room temperature, followed by addition of 5 μl Zenon blocking reagent and incubation at room temperature for 5 min. The conjugated antibodies were applied to samples within 30 min. Cells were then incubated with the conjugated antibodies at 4°C for 20 min, fixed with 300 μl 4% PFA. Events were collected on a modified LSRII flow cytometer (BD Immunocytometry Systems, Franklin Lakes, NJ, USA), and

electronic compensation was performed with antibody capture beads (BD Biosciences, Franklin lakes, NJ, USA) stained separately with antibodies used in the test samples. Data were analyzed using FlowJo Version 9.6 (TreeStar, Ashland, OR, USA).

Statistical analysis

All analysis was performed using two-tailed Student's *t*-test. Differences with $P < 0.05$ were considered statistically significant. Mean ± SEM of triplicated experiments were calculated and presented.

Conflict of Interest statement. The authors have no conflict of interest to disclose.

Funding

This work was supported by the Intramural Research Program (IRP) of the *Eunice Kennedy Shriver* National Institute of Child Health & Human Development (NICHD), National Institutes of Health (NIH), Bethesda, MD 20892, USA.

References

1. Skalhegg, B.S. and Tasken, K. (2000) Specificity in the cAMP/PKA signaling pathway. Differential expression, regulation, and subcellular localization of subunits of PKA. *Front. Biosci.*, **5**, D678–D693.
2. Gamm, D.M., Baude, E.J. and Uhler, M.D. (1996) The major catalytic subunit isoforms of cAMP-dependent protein kinase have distinct biochemical properties in vitro and in vivo. *J. Biol. Chem.*, **271**, 15736–15742.
3. Di Benedetto, G., Zoccarato, A., Lissandron, V., Terrin, A., Li, X., Houslay, M.D., Baillie, G.S. and Zaccolo, M. (2008) Protein kinase A type I and type II define distinct intracellular signaling compartments. *Circ. Res.*, **103**, 836–844.
4. Das, R., Esposito, V., Abu-Abed, M., Anand, G.S., Taylor, S.S. and Melacini, G. (2007) cAMP activation of PKA defines an ancient signaling mechanism. *Proc. Natl. Acad. Sci. USA*, **104**, 93–98.
5. Gonzalez, G.A. and Montminy, M.R. (1989) Cyclic AMP stimulates somatostatin gene transcription by phosphorylation of CREB at serine 133. *Cell.*, **59**, 675–680.
6. Kirschner, L.S., Carney, J.A., Pack, S.D., Taymans, S.E., Giatzakis, C., Cho, Y.S., Cho-Chung, Y.S. and Stratakis, C.A. (2000) Mutations of the gene encoding the protein kinase A type I-alpha regulatory subunit in patients with the carney complex. *Nat. Genet.*, **26**, 89–92.
7. Kirschner, L.S., Sandrini, F., Monbo, J., Lin, J.P., Carney, J.A. and Stratakis, C.A. (2000) Genetic heterogeneity and spectrum of mutations of the *PRKAR1A* gene in patients with the carney complex. *Hum. Mol. Genet.*, **9**, 3037–3046.
8. Kirschner, L.S., Kusewitt, D.F., Matyakhina, L., Towns, W.H. 2nd, Carney, J.A., Westphal, H. and Stratakis, C.A. (2005) A mouse model for the Carney complex tumor syndrome develops neoplasia in cyclic AMP-responsive tissues. *Cancer. Res.*, **65**, 4506–4514.
9. Griffin, K.J., Kirschner, L.S., Matyakhina, L., Stergiopoulos, S., Robinson-White, A., Lenherr, S., Weinberg, W., Claflin, E., Meoli, E., Cho-Chung, Y.S. and Stratakis, C.A. (2004) Down-regulation of regulatory subunit type 1A of protein kinase A leads to endocrine and other tumors. *Cancer. Res.*, **64**, 8811–8815.
10. Meoli, E., Bossis, I., Cazabat, L., Mavrakis, M., Horvath, A., Shiferaw, M., Fumey, G., Perlemoine, K., Muchow, M., Robinson-White, A. *et al.* (2008) Protein kinase A (PKA) effects of an expressed *PRKAR1A* mutation associated with aggressive tumors. *Cancer. Res.*, **68**, 3133–3141.
11. Tsang, K.M., Starost, M.F., Nesterova, M., Boikos, S.A., Watkins, T., Almeida, M.Q., Harran, M., Li, A., Collins, M.T., Cheadle, C. *et al.* (2010) Alternate protein kinase A activity identifies a unique population of stromal cells in adult bone. *Proc. Natl. Acad. Sci. USA*, **107**, 8683–8688.
12. Burton, K.A., Johnson, B.D., Hausken, Z.E., Westenbroek, R.E., Idzerda, R.L., Scheuer, T., Scott, J.D., Catterall, W.A. and McKnight, G.S. (1997) Type II regulatory subunits are not required for the anchoring-dependent modulation of Ca2+ channel activity by cAMP-dependent protein kinase. *Proc. Natl. Acad. Sci. USA*, **94**, 11067–11072.
13. Cummings, D.E., Brandon, E.P., Planas, J.V., Motamed, K., Idzerda, R.L. and McKnight, G.S. (1996) Genetically lean mice result from targeted disruption of the RII beta subunit of protein kinase A. *Nature*, **382**, 622–626.
14. Jones, S.J. and Boyde, A. (1974) The organization and gross mineralization patterns of the collagen fibers in Sharpey fiber bone. *Cell Tissue Res.*, **148**, 83–96.
15. Nishikawa, T., Masuno, K., Tominaga, K., Koyama, Y., Yamada, T., Takakuda, K., Kikuchi, M., Tanaka, J. and Tanaka, A. (2005) Bone repair analysis in a novel biodegradable hydroxyapatite/collagen composite implanted in bone. *Implant. Dent.*, **14**, 252–260.
16. Sun, L., Blair, H.C., Peng, Y., Zaidi, N., Adebanjo, O.A., Wu, X.B., Wu, X.Y., Iqbal, J., Epstein, S., Abe, E. *et al.* (2005) Calcineurin regulates bone formation by the osteoblast. *Proc. Natl. Acad. Sci. USA*, **102**, 17130–17135.
17. Komori, T. (2010) Regulation of osteoblast differentiation by Runx2. *Adv. Exp. Med. Biol.*, **658**, 43–49.
18. Cao, Y., Zhou, Z., de Crombrugghe, B., Nakashima, K., Guan, H., Duan, X., Jia, S.F. and Kleinerman, E.S. (2005) Osterix, a transcription factor for osteoblast differentiation, mediates antitumor activity in murine osteosarcoma. *Cancer. Res.*, **65**, 1124–1128.
19. Shen, J., Hovhannisyan, H., Lian, J.B., Montecino, M.A., Stein, G.S., Stein, J.L. and Van Wijnen, A.J. (2003) Transcriptional induction of the osteocalcin gene during osteoblast differentiation involves acetylation of histones h3 and h4. *Mol. Endocrinol.*, **17**, 743–756.
20. Malaval, L., Liu, F., Roche, P. and Aubin, J.E. (1999) Kinetics of osteoprogenitor proliferation and osteoblast differentiation in vitro. *J. Cell. Biochem.*, **74**, 616–627.
21. Nesterova, M., Yokozaki, H., McDuffie, E. and Cho-Chung, Y.S. (1996) Overexpression of RII beta regulatory subunit of protein kinase A in human colon carcinoma cell induces growth arrest and phenotypic changes that are abolished by site-directed mutation of RII beta. *Eur. J. Biochem.*, **235**, 486–494.
22. Kim, C., Cheng, C.Y., Saldanha, S.A. and Taylor, S.S. (2007) PKA-I holoenzyme structure reveals a mechanism for cAMP-dependent activation. *Cell*, **130**, 1032–1043.
23. Bianco, P., Kuznetsov, S.A., Riminucci, M., Fisher, L.W., Spiegel, A.M. and Robey, P.G. (1998) Reproduction of human fibrous dysplasia of bone in immunocompromised mice by transplanted mosaics of normal and Gsalpha-mutated skeletal progenitor cells. *J. Clin. Invest.*, **101**, 1737–1744.
24. Pavel, E., Nadella, K., Towns, W.H. II and Kirschner, L.S. (2008) Mutation of Prkar1a causes osteoblast neoplasia driven by dysregulation of protein kinase A. *Mol. Endocrinol.*, **22**, 430–440.
25. Karsenty, G., Kronenberg, H.M. and Settembre, C. (2009) Genetic control of bone formation. *Annu. Rev. Cell. Dev. Biol.*, **25**, 629–648.

26. Wu, J.Y., Aarnisalo, P., Bastepe, M., Sinha, P., Fulzele, K., Selig, M.K., Chen, M., Poulton, I.J., Purton, L.E., Sims, N.A., Weinstein, L.S. and Kronenberg, H.M. (2011) Gsα enhances commitment of mesenchymal progenitors to the osteoblast lineage but restrains osteoblast differentiation in mice. *J. Clin. Invest.*, **121**, 3492–3504.
27. Chagin, A.S., Vuppalapati, K.K., Kobayashi, T., Guo, J., Hirai, T., Chen, M., Offermanns, S., Weinstein, L.S. and Kronenberg, H. M. (2014) G-protein stimulatory subunit alpha and Gq/11α G-proteins are both required to maintain quiescent stem-like chondrocytes. *Nat. Commun.*, **5**, 3673.
28. Siddappa, R., Mulder, W., Steeghs, I., van de Klundert, C., Fernandes, H., Liu, J., Arends, R., van Blitterswijk, C. and de Boer, J. (2009) cAMP/PKA signaling inhibits osteogenic differentiation and bone formation in rodent models. *Tissue. Eng. Part A*, **15**, 2135–2143.
29. Koh, A.J., Beecher, C.A., Rosol, T.J. and McCauley, L.K. (1999) 3′, 5′-Cyclic adenosine monophosphate activation in osteoblastic cells: effects on parathyroid hormone-1 receptors and osteoblastic differentiation in vitro. *Endocrinology*, **140**, 3154–3162.
30. Kondo, H., Guo, J. and Bringhurst, F.R. (2002) Cyclic adenosine monophosphate/protein kinase A mediates parathyroid hormone/parathyroid hormone-related protein receptor regulation of osteoclastogenesis and expression of RANKL and osteoprotegerin mRNAs by marrow stromal cells. *J. Bone. Miner. Res.*, **17**, 1667–1679.
31. Weinstein, L.S., Shenker, A., Gejman, P.V., Merino, M.J., Friedman, E. and Spiegel, A.M. (1991) Activating mutations of the stimulatory G protein in the McCune-Albright syndrome. *N. Engl. J. Med.*, **325**, 1688–1695.
32. Schwindinger, W.F., Francomano, C.A. and Levine, M.A. (1992) Identification of a mutation in the gene encoding the alpha subunit of the stimulatory G protein of adenylyl cyclase in McCune-Albright syndrome. *Proc. Natl. Acad. Sci. USA*, **89**, 5152–5156.
33. Yadav, M.C., Simao, A.M., Narisawa, S., Huesa, C., McKee, M.D., Farquharson, C. and Millan, J.L. (2011) Loss of skeletal mineralization by the simultaneous ablation of PHOSPHO1 and alkaline phosphatase function: a unified model of the mechanisms of initiation of skeletal calcification. *J. Bone. Miner. Res.*, **26**, 286–297.
34. Anderson, H.C., Sipe, J.B., Hessle, L., Dhanyamraju, R., Atti, E., Camacho, N.P. and Millan, J.L. (2004) Impaired calcification around matrix vesicles of growth plate and bone in alkaline phosphatase-deficient mice. *Am. J. Pathol.*, **164**, 841–847.
35. Jang, W.G., Kim, E.J., Kim, D.K., Ryoo, H.M., Lee, K.B., Kim, S.H., Choi, H.S. and Koh, J.T. (2012) BMP2 protein regulates osteocalcin expression via Runx2-mediated Atf6 gene transcription. *J. Biol. Chem.*, **287**, 905–915.
36. Kim, Y.J., Kim, H.N., Park, E.K., Lee, B.H., Ryoo, H.M., Kim, S.Y., Kim, I.S., Stein, J.L., Lian, J.B., Stein, G.S. *et al.* (2006) The bone-related Zn finger transcription factor Osterix promotes proliferation of mesenchymal cells. *Gene.*, **366**, 145–151.
37. Karsenty, G. and Wagner, E.F. (2002) Reaching a genetic and molecular understanding of skeletal development. *Dev. Cell.*, **2**, 389–406.
38. Lin, G.L. and Hankenson, K.D. (2011) Integration of BMP, Wnt, and notch signaling pathways in osteoblast differentiation. *J. Cell. Biochem.*, **112**, 3491–3501.
39. Qin, C., Souza, R.D. and Feng, J.Q. (2007) Dentin matrix protein 1 (DMP1): new and important roles for biomineralization and phosphate homeostasis. *J. Dent. Res.*, **86**, 1134–1141.
40. Gluhak-Heinrick, J., Ye, L., Bonewald, L.F., Feng, J.Q., Macdougall, M., Harris, S.E. and Pavlin, D. (2003) Mechanical loading stimulates dentin matrix protein 1 (DMP1) expression in osteocytes in vivo. *J. Bone Miner. Res.*, **18**, 807–817.
41. Narayanan, K., Ramachandran, A., Hao, J., He, G., Park, K.W., Cho, M. and George, A. (2003) Dual functional roles of dentin matrix protein 1. Implications in biomineralization and gene transcription by activation of intracellular Ca2+ store. *J. Biol. Chem.*, **278**, 17500–17508.
42. Dancer, J.Y., Henry, S.P., Bondaruk, J., Lee, S., Ayala, A.G., de Crombrugghe, B. and Czerniak, B. (2010) Expression of master regulatory genes controlling skeletal development in benign cartilage and bone forming tumors. *Hum. Pathol.*, **41**, 1788–1793.
43. Scott, J.D., Glaccum, M.B., Zoller, M.J., Uhler, M.D., Helfman, D.M., McKnight, G.S. and Krebs, E.G. (1987) The molecular cloning of a type II regulatory subunit of the cAMP-dependent protein kinase from rat skeletal muscle and mouse brain. *Proc. Natl. Acad. Sci. USA*, **84**, 5192–5196.
44. Steagall, W.K., Kelley, T.J., Marsick, R.J. and Drumm, M.L. (1998) Type II protein kinase A regulates CFTR in airway, pancreatic, and intestinal cells. *Am. J. Physiol.*, **274**, 819–826.
45. Brandon, E.P., Logue, S.F., Adams, M.R., Qi, M., Sullivan, S.P., Matsumoto, A.M., Dorsa, D.M., Wehner, J.M., McKnight, G.S. and Idzerda, R.L. (1998) Defective motor behavior and neural gene expression in RIIbeta-protein kinase A mutant mice. *J. Neurosci.*, **18**, 3639–3649.
46. Mantovani, G., Bondioni, S., Alberti, L., Gilardini, L., Invitti, C., Corbetta, S., Zappa, M.A., Ferrero, S., Lania, A.G., Bosari, S. *et al.* (2009) Protein kinase A regulatory subunits in human adipose tissue: decreased R2B expression and activity in adipocytes from obese subjects. *Diabetes*, **58**, 620–626.
47. Zhong, H., Sia, G.M., Sato, T.R., Gray, N.W., Mao, T., Khuchua, Z., Huganir, R.L. and Svoboda, K. (2009) Subcellular dynamics of type II PKA in neurons. *Neuron.*, **62**, 363–374.
48. Stratakis, C.A. (2014) E pluribus unum? The main protein kinase A catalytic subunit (PRKACA), a likely oncogene, and cortisol-producing tumors. *J. Clin. Endocrinol. Metab.*, **99**, 3629–3633.
49. Yin, Z., Pringle, D.R., Jones, G.N., Kelly, K.M. and Kirschner, L. S. (2011) Differential role of PKA catalytic subunits in mediating phenotypes caused by knockout of the Carney complex gene Prkar1a. *Mol. Endocrinol.*, **25**, 1786–1793.
50. Howe, D.G., Wiley, J.C. and McKnight, G.S. (2002) Molecular and behavioral effects of a null mutation in all PKA C beta isoforms. *Mol. Cell. Neurosci.*, **20**, 515–524.
51. Skålhegg, B.S., Huang, Y., Su, T., Idzerda, R.L., McKnight, G.S. and Burton, K.A. (2002) Mutation of the Calpha subunit of PKA leads to growth retardation and sperm dysfunction. *Mol. Endocrinol.*, **16**, 630–639.
52. Lodish, M.B., Yuan, B., Levy, I., Braunstein, G.D., Lyssikatos, C., Salpea, P., Szarek, E., Karageorgiadis, A.S., Belyavskaya, E., Raygada, M. *et al.* (2015) Germline PRKACA amplification causes variable phenotypes that may depend on the extent of the genomic defect: molecular mechanisms and clinical presentations. *Eur. J. Endocrinol.*, **172**, 803–811.
53. Berthon, A.S., Szarek, E. and Stratakis, C.A. (2015) PRKACA: the catalytic subunit of protein kinase A and adrenocortical tumors. *Front Cell Dev Biol.*, **3**, 26.
54. Forlino, A., Vetro, A., Garavelli, L., Ciccone, R., London, E., Stratakis, C.A. and Zuffardi, O. (2014) *PRKACB* and Carney complex. *N. Engl. J. Med.*, **370**, 1065–1067.
55. Livak, K.J. and Schmittgen, T.D. (2001) Analysis of relative gene expression data using real-time quantitative PCR and the 2(-Delta Delta C(T)) Method. *Methods*, **25**, 402–408.